

# RSC Advances



This is an *Accepted Manuscript*, which has been through the Royal Society of Chemistry peer review process and has been accepted for publication.

*Accepted Manuscripts* are published online shortly after acceptance, before technical editing, formatting and proof reading. Using this free service, authors can make their results available to the community, in citable form, before we publish the edited article. This *Accepted Manuscript* will be replaced by the edited, formatted and paginated article as soon as this is available.

You can find more information about *Accepted Manuscripts* in the [Information for Authors](#).

Please note that technical editing may introduce minor changes to the text and/or graphics, which may alter content. The journal's standard [Terms & Conditions](#) and the [Ethical guidelines](#) still apply. In no event shall the Royal Society of Chemistry be held responsible for any errors or omissions in this *Accepted Manuscript* or any consequences arising from the use of any information it contains.



## Textile/ $\text{Al}_2\text{O}_3$ - $\text{TiO}_2$ Nanocomposite as an Antimicrobial and Radical Scavenger Wound Dressing

Shokoh Parham,<sup>a</sup> Sheela Chandren,<sup>a</sup> Dedy H.B. Wicaksono,<sup>b,c</sup> Saeedeh Bagherbaigi,<sup>b</sup> Siew Ling Lee,<sup>a</sup> Lai Sin Yuan,<sup>a</sup> and Hadi Nur<sup>\*a</sup>

Improving the antimicrobial activity and radical scavenging ability of textile-based nanocomposite (textile/ $\text{TiO}_2$ , textile/ $\text{Al}_2\text{O}_3$ / $\text{TiO}_2$ , textile/ $\text{Al}_2\text{O}_3$  and textile/ $\text{Al}_2\text{O}_3$ - $\text{TiO}_2$  bimetal oxide nanocomposite) is the key issue in developing good and flexible wound dressing. In this work, flexible textile attached with  $\text{Al}_2\text{O}_3$ - $\text{TiO}_2$  nanoparticles was prepared by dipping the textile in a suspension containing  $\text{Al}_2\text{O}_3$ - $\text{TiO}_2$  nanoparticles (150 mmole/L). The mean radical scavenging ability for textile/ $\text{TiO}_2$ , textile/ $\text{Al}_2\text{O}_3$ / $\text{TiO}_2$ , textile/ $\text{Al}_2\text{O}_3$  and textile/ $\text{Al}_2\text{O}_3$ - $\text{TiO}_2$  bimetal oxide nanocomposite as measured by liquid ultraviolet visible spectroscopy (UV-Vis) coupled with dependence formula were 0.2%, 35.5%, 35.0% and 38.2%, respectively. Based on the X-ray diffraction (XRD) patterns, the preface reactive oxygen species (ROS) scavenging ability shown by the textile/ $\text{Al}_2\text{O}_3$ - $\text{TiO}_2$  bimetal oxide nanocomposite is most probably caused by the crystal structure concluding corundum-like structure, with  $\text{Al}^{3+}$  ions filling the octahedral sites in the lattice. Increased antimicrobial activity measured by optical density at 600 nm recorded for textile/ $\text{Al}_2\text{O}_3$ - $\text{TiO}_2$  bimetal oxide nanocomposite showed better interaction between  $\text{Al}_2\text{O}_3$  and  $\text{TiO}_2$  nanoparticle. This good interaction is expected to lead to better antimicrobial and radical scavenging ability as shown by the *E. coli* and Human Skin Fibroblast (HSF) cytotoxicity tests, respectively.

Received 00th January 20xx,  
Accepted 00th January 20xx

DOI: 10.1039/x0xx00000x

www.rsc.org/

### 1. Introduction

Wound dressings are usually designed to be in direct contact with the wound, in order to prevent further harm and support healing. The main difference between wound dressings and bandages is that bandages are mainly used to hold a wound dressing in place while wound dressings contribute to the healing process. Many types of wound dressing already exist in market, such as fabric, spider webs, manure, leaves and honey.<sup>1</sup> Currently, the most commonly used wound dressings materials are gauze, films, gels, foams, hydrocolloids, alginates, hydrogels, polysaccharides beads, pasta and granules.<sup>2</sup> In wound dressing materials, a layer of non-sticking film over the absorbent material is added in order to prevent direct adhesion to the wound.<sup>3</sup>

Parallel to immediate improvement of wound dressings, control of microorganism's harmful effects would be necessary.<sup>4</sup> A broad range of microorganisms can coexist in natural equilibrium with human body and living environments. This uncontrolled fast thriving of microbes can lead to some serious problems, such as dangerous infected wound.<sup>4</sup>

Recently, the use of nanoparticles in clinical and experimental settings has increased due to their wide range of biomedical applications, for example in wound healing, imaging and drug delivery. The antimicrobial ability and nontoxicity are two key factors for biomedical applications like wound healing. In this context, it is widely accepted that cytotoxicity to human or animal cells depends on some parameters such as mechanism of antimicrobial action. However, recent literature suggests that cytotoxicity of some nanoparticles such as  $\text{TiO}_2$ , Ag and ZnO is related to oxidative stress. This toxicity is related to the generation of reactive oxygen species (ROS) free radicals. Previous researchers also reported that the toxicity of  $\text{Al}_2\text{O}_3$  is not high because of its role as radical scavenger. Therefore it can block ROS generation.<sup>5,6</sup>

Generally, antimicrobial agents are used to prevent the harmful effects of microorganisms. Most of the existing wound dressing uses textile.<sup>8</sup> Antimicrobial agents are attached on textiles to prevent the undesirable effects of textiles, such as the degradation phenomena of staining, deterioration and coloring of fibers.<sup>7</sup> Due to their dye degradation potential, even some fungus can be used to remove dyes,<sup>8</sup> unpleasant odors,<sup>9</sup> and decrease the potential health risks of textiles.<sup>10</sup>

Conventional textile wound dressings, however, do not possess any resistance towards microorganisms and materials generated from their metabolism.<sup>4</sup> They are most commonly prone to multiplication, proliferation and accumulation of microorganisms into their surrounding environment.<sup>11</sup> In fact, several factors such as temperature, humidity and presence of

<sup>a</sup> Centre for Sustainable Nanomaterials, Ibnu Sina Institute for Scientific and Industrial Research, Universiti Teknologi Malaysia, 81310 UTM Skudai, Johor, Malaysia. E-mail: hadi@kimia.fs.utm.my

<sup>b</sup> Medical Devices and Technology Research Group (MediTeg), Faculty of Biosciences and Medical Engineering, Universiti Teknologi Malaysia, 81310 UTM Skudai, Johor, Malaysia.

<sup>c</sup> IJN-UTM Cardiovascular Engineering Centre, Faculty of Biosciences and Medical Engineering, Universiti Teknologi Malaysia, 81310 UTM Skudai, Johor, Malaysia.

materials on the textile's surfaces can make the textile an optimal enrichment culture for a rapid multiplication of microorganisms.<sup>12</sup> Therefore, the control of these terrible effects is necessary.

Based on the above reasons, the high antimicrobial property of textile wound dressings is necessary. This can be achieved by, the use of metal oxide nanoparticles such as titania (TiO<sub>2</sub>) and silver oxide (AgO), as they are known to possess strong antimicrobial properties.<sup>13</sup> Apart from these metal oxides, alumina (Al<sub>2</sub>O<sub>3</sub>) nanoparticles have wide-range applications in industries, however, Al<sub>2</sub>O<sub>3</sub> lacks strong antimicrobial activity.<sup>23</sup> When metal oxide is a base for mixed oxide, therefore mixed oxide may be able to be used as antimicrobial agents. Zirconia (ZrO<sub>2</sub>), Al<sub>2</sub>O<sub>3</sub>, silica (SiO<sub>2</sub>) and TiO<sub>2</sub> are some of the base for making mixed metal oxide supports. Different kinds of mixed metal oxides have been reported such as ZrO<sub>2</sub>-TiO<sub>2</sub>, TiO<sub>2</sub>-SiO<sub>2</sub> and Al<sub>2</sub>O<sub>3</sub>-SiO<sub>2</sub>.<sup>14</sup>

Currently, nanosized inorganic and organic nanoparticles are finding increasing applications in medical devices, e.g. as antimicrobial agents due to their ability to be biologically functionalized.<sup>15</sup> Antimicrobial agents have a lot of industrial applications in health care, medical care, synthetic textiles and environmental products.<sup>16,17</sup> Antibacterial activity is known to be a function of the surface area in contact with the microorganisms; therefore a larger surface area (as in the case of nanoparticles) shows a broader range of probable reactions with bioorganic present on the cell surface, such as environmental organic and inorganic species.<sup>18</sup> However, the antimicrobial activity of these nanoparticles can produce ROS free radicals, which are toxic to human cell. Previous studies on the toxicity of metal oxide nanoparticles to bacterial species are limited, even though their bactericidal properties have been reported in same biomedical literatures.<sup>19</sup>

Radical scavenging ability can decrease the toxicity of metal oxide to human cell. A scavenger is a chemical substance added to a mixture in order to deactivate or remove unwanted and impurities reaction products, such as oxygen, so as to avoid any unfavorable reactions.<sup>20</sup> Metal oxides are generally toxic to microbes in the environment.<sup>19</sup> It has been shown that nanoparticles with positive charge such as zinc oxide could bind the gram-negative cell membrane by electrostatic attraction.<sup>20</sup> Clearly, the intimate relationship between the physicochemistry of the medium and membrane biology of the microbe is emerging as a key factor in nanoparticles toxicity to microorganisms.<sup>21</sup>

Only a few studies have been carried out on the interaction of the Al<sub>2</sub>O<sub>3</sub> and Al<sub>2</sub>O<sub>3</sub>-TiO<sub>2</sub> bimetal oxide with microbes. One study found no detrimental effect of Al<sub>2</sub>O<sub>3</sub> slurry between 62.5 and 250 mg/L concentration range on *E. coli*.<sup>22</sup> Past literatures have reported the toxicity and harmful effects of other antimicrobial agents.<sup>23</sup> The purpose of the current study is to improve the antimicrobial properties of textile as wound dressing without being toxic to human cell. This paper focuses on the synthesis and characterization of textile/Al<sub>2</sub>O<sub>3</sub> nanocomposite, textile/TiO<sub>2</sub> nanocomposite textile/Al<sub>2</sub>O<sub>3</sub>/TiO<sub>2</sub> nanocomposite and textile/Al<sub>2</sub>O<sub>3</sub>-TiO<sub>2</sub> bimetal oxide nanocomposite as wound dressings. The antimicrobial

properties and radical scavenging ability of these nanocomposites were also tested. The antimicrobial mechanism of these nanocomposites is also suggested.

## 2. Materials and methods

### 2.1. Reagents

The materials used in this study were citric acid (C<sub>6</sub>H<sub>8</sub>O<sub>7</sub>-H<sub>2</sub>O, QReC), aluminium nitrate (Al(NO<sub>3</sub>)<sub>3</sub>·9H<sub>2</sub>O, QReC), sodium carbonate (Na<sub>2</sub>CO<sub>3</sub>, QReC), titanium isopropoxide (C<sub>12</sub>H<sub>28</sub>O<sub>4</sub>Ti, Merck), ethyl acetoacetate (C<sub>6</sub>H<sub>10</sub>O<sub>3</sub>, Merck), ethanol (C<sub>2</sub>H<sub>6</sub>O, Merck), hydrochloric acid (HCl, 96%, Merck), textile (100% cotton (White plain weave cotton textile (Mirota Batik, Surabaya, Indonesia, unmercerized, bleached, having 126 denier, or 14 mg m<sup>-2</sup> and a fabric count of 95 × 95, with a mass density of 9.3 mg cm<sup>-2</sup>, and 160 fibers per inch), sodium hydroxide (NaOH 7%Wt, Merck) and sulfuric acid (H<sub>2</sub>SO<sub>4</sub> 96%, Merck). The bactericidal experiments were carried out with gram-negative bacteria *Escherichia coli* (*E. coli*) (strain.DH5D-*E. coli*) in Luria Bertani (LB) medium (Himedia Laboratories Ltd). Tryptone or peptone (Sigma Aldrich), yeast extract (Sigma Aldrich), agar (Sigma Aldrich) were also used. The cytotoxicity test was carried out with Human Skin Fibroblast (HSF 1184 catalogue no. 90011883, available from ECACC, United Kingdom). The Minimum Essential Media (MEM) (catalogue no. 11095, Invitrogen), Fetal Bovine Serum (FBS) (Sigma Aldrich), Penicillin Streptomycin (PS) (Sigma Aldrich), PBS (Phosphate Buffered Saline Solutions) (Sigma Aldrich), Trypsin/EDTA (Invitrogen), Hank's Balanced Salt Solution (HBSS) (Sigma Aldrich) and <sup>TM</sup> Red CMTPX dye (Sigma Aldrich) were also used.

### 2.2. Textile preparation

Before the synthesis of the textile-based nanocomposite, the wax on the textile's surface was removed by sodium carbonate (Na<sub>2</sub>CO<sub>3</sub>). First, Na<sub>2</sub>CO<sub>3</sub> (10 mg) and water as solvent (25 ml) was added to textile (1.5 g) in a beaker. The mixture was boiled for 5 min at 100 °C. After that, the mixture was washed with deionized water until the pH was 6–7 and then the sample was dried in air.<sup>24</sup> The weight of the textile used was 1.5 g.

### 2.3. Synthesis of textile/Al<sub>2</sub>O<sub>3</sub> nanocomposite

The alumina nanoparticles were synthesized by using the sol gel method. Al(NO<sub>3</sub>)<sub>3</sub>·9H<sub>2</sub>O was added to citric acid. Then this mixture was dissolved in deionized water and stirred at 80 °C for 8 h. After that the yellowish residue was collected. The obtained sample was calcined in a furnace at 1100 °C for 2 h. The sample was then weighed and the data were collected.<sup>25</sup> The synthesis of textile/Al<sub>2</sub>O<sub>3</sub> nanocomposite was done by functionalizing the prepared Al<sub>2</sub>O<sub>3</sub> on textile. Textile (1.5 g) was soaked in a solution of Al<sub>2</sub>O<sub>3</sub> nanoparticles (150 mmole/L), with NaOH solution (7 wt %) as the solvent. The solution was stirred for 24 h and then immersed in a H<sub>2</sub>SO<sub>4</sub> (5wt %) water bath at 15 °C immediately for neutralization. After neutralization, the sample was washed with deionized water

to remove the solvent. The sample was then dried in room temperature.

#### 2.4. Synthesis of textile/TiO<sub>2</sub> nanocomposite

TiO<sub>2</sub> nanoparticle was also synthesis by using the sol gel method. First, C<sub>16</sub>H<sub>36</sub>O<sub>4</sub>Ti (1 ml) and C<sub>2</sub>H<sub>5</sub>OH (5 ml) were added in a clean vial (10 ml). Then the solution was stirred at room temperature for 6 h. After that, deionized water (0.3 ml) and HCl (0.4 ml) were added before stirring the solution for 1 h. The obtained sample is dried in oven at 80 °C and then it was calcined at 800 °C for 2 h.<sup>27</sup> The synthesis of textile/TiO<sub>2</sub> nanocomposite was done by functionalizing the prepared TiO<sub>2</sub> on textile. Textile (1.5 g) was soaked in a solution of TiO<sub>2</sub> nanoparticles (150 mmole/L), with NaOH solution (7 wt %) as the solvent. The solution was stirred for 24 h and then the solution was immersed in a H<sub>2</sub>SO<sub>4</sub> (5wt %) water bath at 15 °C immediately for neutralization. After neutralization, the sample was washed with deionized water to remove the solvent. The sample was then dried in room temperature.

#### 2.5. Synthesis of textile /Al<sub>2</sub>O<sub>3</sub>-TiO<sub>2</sub> nanocomposite

The Al<sub>2</sub>O<sub>3</sub>-TiO<sub>2</sub> bimetal oxide nanoparticles were firstly synthesized by using sol gel method. Al(NO<sub>3</sub>)<sub>3</sub>·9H<sub>2</sub>O added to ethanol, C<sub>2</sub>H<sub>5</sub>OH (20 ml) and C<sub>6</sub>H<sub>10</sub>O<sub>3</sub> (ethyl acetoacetate) (30ml) was added as a solvent. Then the solution was stirred at room temperature for 30 min. After that C<sub>12</sub>H<sub>28</sub>O<sub>4</sub>Ti was added to obtain a solution such that the final composition contains 30 wt%TiO<sub>2</sub>-70 wt% Al<sub>2</sub>O<sub>3</sub>. Distilled water was then added to complete the hydrolysis reaction.

The solution was further stirred for 2 h and then heated at 80 °C. The obtained sample was then dried and calcined at 500 °C (2h) and 1100 °C (2 h). The synthesis of textile/Al<sub>2</sub>O<sub>3</sub> -TiO<sub>2</sub> bimetal oxide nanocomposite was done by functionalizing Al<sub>2</sub>O<sub>3</sub>-TiO<sub>2</sub> nanoparticles on to the textile. Textile (1.5 g), Al<sub>2</sub>O<sub>3</sub>-TiO<sub>2</sub> bimetal oxide nanoparticle (150 mmole/L), and NaOH solution ((7 wt %) as the solvent) were mixed and stirred for 24 h. Then the solution was immersed in H<sub>2</sub>SO<sub>4</sub> (5wt %) water bath at 15 °C for neutralization. After neutralization, the sample was washed with deionized water to remove the solvent. The sample was then dried in room temperature.

**Table 1** Codes and preparation methods of the samples.

Code	Treatment/Preparation method
Al <sub>2</sub> O <sub>3</sub>	Sol-gel
TiO <sub>2</sub>	Sol-gel
Al <sub>2</sub> O <sub>3</sub> -TiO <sub>2</sub>	Sol-gel
Al <sub>2</sub> O <sub>3</sub> /TiO <sub>2</sub>	physical mixing
textile/Al <sub>2</sub> O <sub>3</sub>	functionalized with Al <sub>2</sub> O <sub>3</sub>
textile/TiO <sub>2</sub>	functionalized with TiO <sub>2</sub>
textile/Al <sub>2</sub> O <sub>3</sub> -TiO <sub>2</sub>	functionalized with Al <sub>2</sub> O <sub>3</sub> -TiO <sub>2</sub>
textile/Al <sub>2</sub> O <sub>3</sub> /TiO <sub>2</sub>	functionalized with physically-mixed Al <sub>2</sub> O <sub>3</sub> /TiO <sub>2</sub>

#### 2.6. Synthesis of textile /Al<sub>2</sub>O<sub>3</sub>/TiO<sub>2</sub> nanocomposite

Synthesis of textile/Al<sub>2</sub>O<sub>3</sub>/TiO<sub>2</sub> nanocomposite was done by functionalizing Al<sub>2</sub>O<sub>3</sub> and TiO<sub>2</sub> nanoparticles on textile. First Al<sub>2</sub>O<sub>3</sub> and TiO<sub>2</sub> nanoparticles were mixed physically and then the textile (1.5 g) was soaked in a solution of solution of Al<sub>2</sub>O<sub>3</sub> and TiO<sub>2</sub> nanoparticles. The solution was then stirred for 24h and then the sample was dried in room temperature. The codes and preparation methods of the samples are given in Table 1.

#### 2.7. Growth inhibition study

The inhibitory growth of bacteria, defined as the concentration of material that inhibits the growth of bacteria, was determined based on batch cultures containing of textile/Al<sub>2</sub>O<sub>3</sub> nanocomposite, textile/Al<sub>2</sub>O<sub>3</sub>/TiO<sub>2</sub> nanocomposite (150 mmol/L) and textile/Al<sub>2</sub>O<sub>3</sub>-TiO<sub>2</sub> nanocomposite (75, 100, 125 and 150 mmol/L). Sterile side-arm Erlenmeyer flasks (250 ml) containing 50 mL of liquid broth culture (LB medium) were sonicated for 10 min after the addition of the nanocomposite to prevent aggregation. Subsequently, the flasks were inoculated with 1 ml of the freshly prepared bacterial suspension to maintain initial bacterial concentration with the role of 108 colony-forming units per millilitre, and then incubated in an orbital shaker with the speed of 200 rpm at 30 °C. The high rotary shaking speed was selected to minimize aggregation and settlement of the sample over the incubation period. Lower speed setting during incubation might cause underestimation of the antimicrobial activity of the sample. Bacterial growth was measured as the increase in absorbance at 600 nm determined using a spectrophotometer (CL-157 colorimeter; ELICO Company, Hyderabad, India). The experiments also included a positive control with a flask containing nanocomposite and nutrient medium, while the negative control was done with a flask containing textile without Al<sub>2</sub>O<sub>3</sub> or TiO<sub>2</sub> and medium. The negative controls are used to indicate the microbial growth profile in the absence of nanocomposite. The absorbance values for positive controls were subtracted from the experimental values (flasks containing medium and nanocomposite).<sup>26</sup>

#### 2.8. Characterization

The structural characterizations were performed by an X-ray diffractometer (XRD) (Bruker AXS D8 Advanced) using Cu K $\alpha$  radiations ( $k = 1.54178 \text{ \AA}$ ) at 40 kV and 10 mA in the range of 5–80°, scanning speed of 2 min<sup>-1</sup> and resolution of 0.011. Fourier transform infrared (FTIR) spectroscopy was performed by a Nexus 670 Spectrometer (Nicolet, USA) in order to identify structural features of the heat treated powders. Measurements were conducted in the wavelength range of 4000–400 cm<sup>-1</sup>. All samples for FTIR measurement were mixed well with potassium bromide (KBr) in the weight ratio of 1:100 and then pressed into translucent pellets. A field-emission scanning electron microscope equipped with an energy dispersion X-ray spectrometer (FESEM-EDX) (JEOL JSM-6701 F) was used to observe the morphology as well as to obtain the elemental analysis of the samples. Prior to analysis, the

samples were coated with gold (Au) by sputtering technique. The radical scavenging ability of the samples was measured by using a Shimadzu 1800 UV-visible spectrophotometer in the range of 250–800 nm.

### 2.9. Assay of scavenging activity

For the scavenging activity testing, the nanocomposites were added to the culture of *E.coli* (20 mL). The solution was shaken for 14 h at 37 °C in a shaker. The absorbances of the samples and control were determined by a UV/Vis spectrophotometer at 325 nm after 14 h. The curve was made based on the absorbance value. Scavenging activity was calculated using the following equation:<sup>27</sup>

$$S_a (\%) = \left( \frac{A_s - A_b}{A_b} \right) \times 100 \quad (1)$$

Where  $S_a$  is the scavenging activity of tested sample (%),  $A_b$  is the absorbance of the control and  $A_s$  is the absorbance in the presence of the tested sample.

### 2.10. Metal release analysis

All samples (textile/ $\text{Al}_2\text{O}_3$  nanocomposite, textile/ $\text{TiO}_2$  nanocomposite, textile/ $\text{Al}_2\text{O}_3$ - $\text{TiO}_2$  nanocomposite and textile/ $\text{Al}_2\text{O}_3$ / $\text{TiO}_2$  nanocomposite and textile) were added in distilled water (20 ml) and kept 14 h, after which the nanocomposite were removed by centrifugation. The release of the inorganic content from the textile was analysed by Inductively Coupled Plasma Mass Spectrometry (ICP-MS).

### 2.11. Cell culture test

Human Skin Fibroblast, HSF (cell size of 12  $\mu\text{m}$ ) was cultured according to the Freshney protocol. The cells were cultured in MEM with 2 mM Glutamine, 1% (v/v) PS and 10% (v/v) FBS. The attached cell cultures were maintained at specified cells concentrations of  $2\text{--}9 \times 10^5$  cells/ml in a humidified incubator (5%  $\text{CO}_2$  at 37 °C). A confluence stage of cell reached within 72 hour. The cells passages were used; (P11 – P15). The cells were washed by PBS while the cells are about 80% confluent. They were later detached by using 0.25% Trypsin/EDTA. In order to obtain cells pellets the cells were centrifuged at 2100 rpm for 5 min. The cells suspensions were used in 3 ml of MEM with a concentration of  $5 \times 10^5$  cells/ml. Finally the cell is stained by <sup>TM</sup>Red CMTPX dye. The HSF cells in 12-well plates with or without samples were inserted into each well, 24 h before each experiment.

## 3. Results and discussion

### 3.1. Crystallinities and structure

The XRD pattern for  $\text{Al}_2\text{O}_3$ / $\text{TiO}_2$  nanoparticles prepared by physical mixing of  $\text{TiO}_2$  (calcined at 800 °C) and  $\text{Al}_2\text{O}_3$  (calcined at 1100 °C) for 2 h shown in Fig. 1 (a) show mixed peaks of  $\text{Al}_2\text{O}_3$  in the  $\alpha$  structure and  $\text{TiO}_2$  in the rutile form. The XRD patterns for  $\text{TiO}_2$  (calcined at 800 °C) and  $\text{Al}_2\text{O}_3$  (calcined at 1100 °C) are shown in Fig. 1 (b) and (d), respectively.  $\text{Al}_2\text{O}_3$  is in the  $\alpha$  structure (corundum-like structure, where the oxygen

atoms adopted hexagonal close-packing and  $\text{Al}^{3+}$  ions filling two thirds of the octahedral sites in the lattice) (ICDD 00-046-1212), while  $\text{TiO}_2$  is in the rutile form (PDF-00-21-1276). It has been reported that the  $\alpha$  structure of can act as radical scavenger.<sup>28</sup> The XRD patterns for  $\text{Al}_2\text{O}_3$ - $\text{TiO}_2$  nanoparticles prepared by sol-gel method and calcined at 1100 and 500 °C for 2 h are shown in Fig. 1(c) and (e), respectively. When calcination was carried out at 500 °C, the  $\text{Al}_2\text{O}_3$ - $\text{TiO}_2$  nanoparticles were in the amorphous phase. Calcination at 1100 °C turned the  $\text{Al}_2\text{O}_3$ - $\text{TiO}_2$  nanoparticles into crystalline phase.

The eight main peaks of this nanoparticle are at  $2\theta$  value of 25.78°, 35.15°, 43.35°, 52.54°, 57.49°, 61.29°, 68.21°, 77.22°, which are characterize of the  $\alpha$ - $\text{Al}_2\text{O}_3$  (ICDD 00-046-1212). The peaks at around 34.45°, 48.62°, 50.07°, 59.93° are attributed to  $\text{Al}_2\text{TiO}_5$  (PDF-18-0068), while the peaks at around 27.44°, 36.08°, 56.64°, 64.03°, 65.47° are from rutile  $\text{TiO}_2$  (PDF-21-1276).

**Table 2** The XRD peak intensity percentage for  $\text{Al}_2\text{O}_3$ - $\text{TiO}_2$  nanoparticles (1100 °C).

Peak ( $2\theta$ (°))	Compound	%
25.78	$\alpha$ - $\text{Al}_2\text{O}_3$	66.3
35.15	$\alpha$ - $\text{Al}_2\text{O}_3$	86.4
43.35	$\alpha$ - $\text{Al}_2\text{O}_3$	100
52.54	$\alpha$ - $\text{Al}_2\text{O}_3$	32.8
57.49	$\alpha$ - $\text{Al}_2\text{O}_3$	88.1
61.29	$\alpha$ - $\text{Al}_2\text{O}_3$	15.5
68.21	$\alpha$ - $\text{Al}_2\text{O}_3$	56.3
77.22	$\alpha$ - $\text{Al}_2\text{O}_3$	24.6
27.44	R- $\text{TiO}_2$	51.5
36.08	R- $\text{TiO}_2$	50.1
56.64	R- $\text{TiO}_2$	27.2
64.03	R- $\text{TiO}_2$	28.1
65.47	R- $\text{TiO}_2$	39.4
34.45	$\text{Al}_2\text{TiO}_5$	48.1
48.62	$\text{Al}_2\text{TiO}_5$	27.4
50.07	$\text{Al}_2\text{TiO}_5$	44.7
59.93	$\text{Al}_2\text{TiO}_5$	14.3



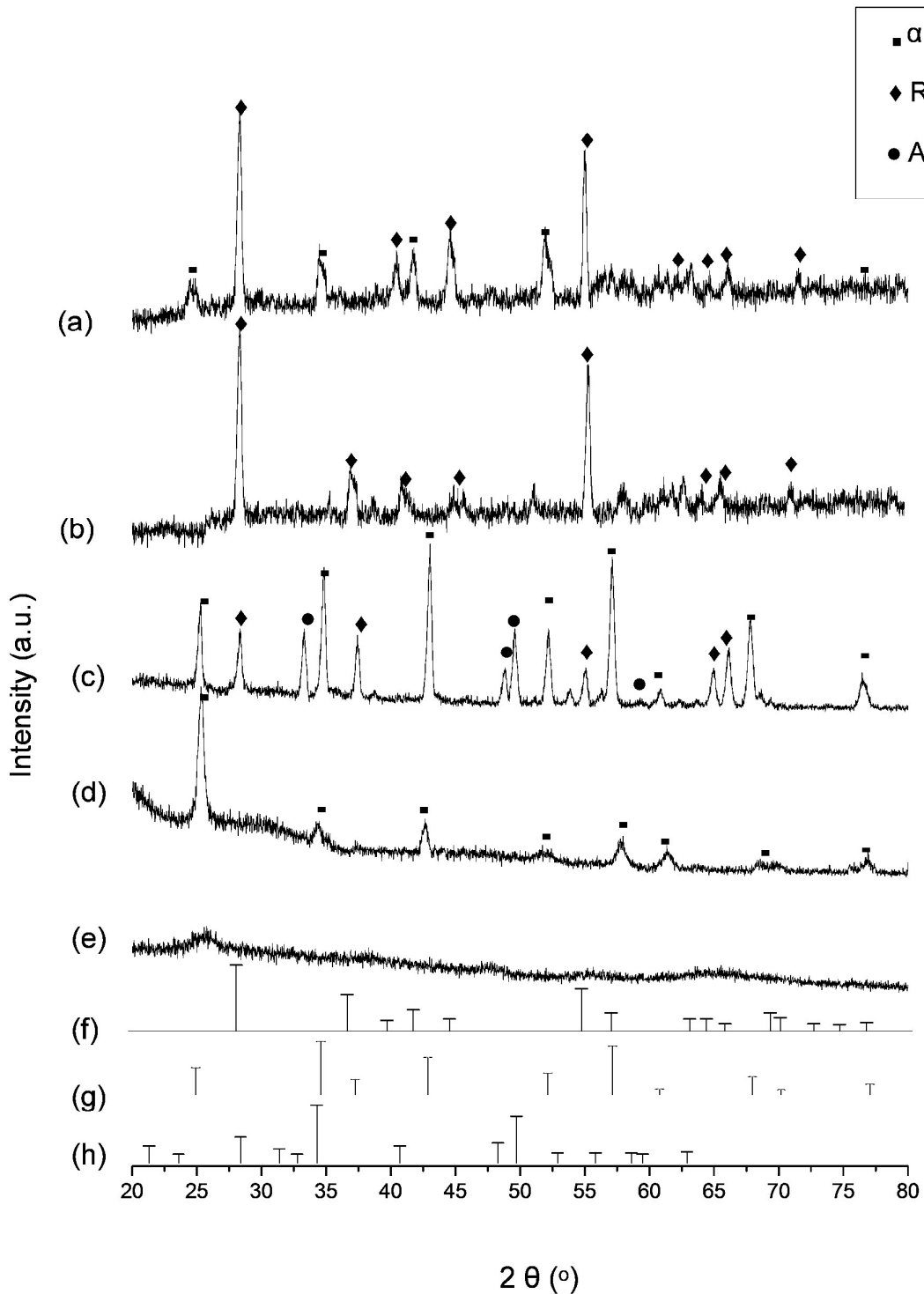


**Fig. 1** XRD patterns for (a) Al<sub>2</sub>O<sub>3</sub>/TiO<sub>2</sub> (b) TiO<sub>2</sub> nanoparticles (c) Al<sub>2</sub>O<sub>3</sub>-TiO<sub>2</sub> nanoparticles (1100 °C) (d) Al<sub>2</sub>O<sub>3</sub> nanoparticles, (e) Al<sub>2</sub>O<sub>3</sub>-TiO<sub>2</sub> nanoparticles (500 °C), (f) TiO<sub>2</sub> nanoparticles (PDF-21-1276), (g) Al<sub>2</sub>O<sub>3</sub> (ICDD 00-046-1212), (h) Al<sub>2</sub>TiO<sub>5</sub> (PDF-18-0068).

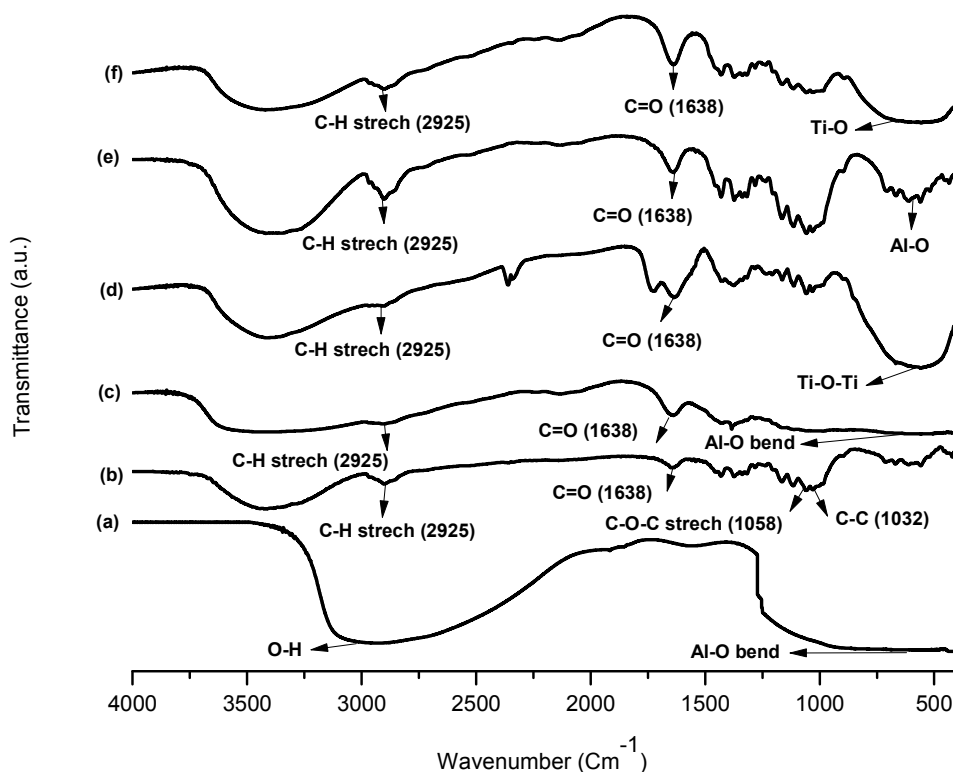


**Fig. 2** FTIR spectra of (a)  $\text{Al}_2\text{O}_3$ - $\text{TiO}_2$  nanoparticles, (b) textile, (c) textile/ $\text{Al}_2\text{O}_3$ - $\text{TiO}_2$ /textile nanocomposite, (d) textile/ $\text{Al}_2\text{O}_3$ / $\text{TiO}_2$  nanocomposite, (e) textile/ $\text{Al}_2\text{O}_3$  nanocomposite and (f) textile/ $\text{TiO}_2$  nanocomposite.

The crystal structure of  $\text{Al}_2\text{O}_3$ - $\text{TiO}_2$  bimetal oxide nanoparticles obtained in this research is different from the previously reported structure of this metal oxide,<sup>29</sup> which was  $\beta$ - $\text{Al}_2\text{TiO}_5$ , which has a pseudobrookite crystal structure (orthorhombic lattice). In this structure, each  $\text{Al}^{3+}$  or  $\text{Ti}^{4+}$  cation is surrounded by six oxygen ions forming distorted oxygen octahedral. These  $\text{AlO}_6$  or  $\text{TiO}_6$  octahedral forms oriented by double chains weakly bonded by shared edges. This structural feature is responsible for the strong thermal expansion anisotropy and may induce strong antimicrobial activity.<sup>30</sup>

But this structure does not have any free capacity to scavenge oxygen free radicals. Therefore, although  $\beta$ - $\text{Al}_2\text{TiO}_5$  have shown antimicrobial activity (based on the oxidation ability), it cannot act as a radical scavenger.<sup>31</sup> Table 2 shows that the highest peak percentages came from  $\alpha$ - $\text{Al}_2\text{O}_3$  while the lowest peak percentages are from  $\text{Al}_2\text{TiO}_5$  (based on Fig. 1(C)).

### 3.2. Functional groups

The FTIR spectra for the samples are shown in Fig. 2. The characteristic peaks for the stretching vibrations of OH groups can be seen at about  $3132$ – $3472$   $\text{cm}^{-1}$  for all the samples which is connected to the sol-gel synthesis.<sup>32</sup> The hydrogen

bonding between the particles of  $\text{Al}_2\text{O}_3$ - $\text{TiO}_2$  caused a shift in the O-H towards a higher wavenumber from  $3132$ – $3472$  to  $3432$ – $3672$   $\text{cm}^{-1}$  (Fig. 2(a) and 2(c)). In the FTIR spectra of  $\text{Al}_2\text{O}_3$ - $\text{TiO}_2$  nanoparticles (Fig. 2(a)), bands due to the stretching vibrations of Al-O bonds of the octahedral coordinated Al were observed in the range of  $500$ – $750$   $\text{cm}^{-1}$ .<sup>33</sup> In the spectra of this sample, peaks corresponding to the Ti-O bond vibrations occur in the range of  $594$ – $639$   $\text{cm}^{-1}$ . However the FTIR spectra of textile/ $\text{Al}_2\text{O}_3$ - $\text{TiO}_2$  and textile/ $\text{Al}_2\text{O}_3$ / $\text{TiO}_2$  nanocomposites are different. This difference is caused by the bonded of  $\text{TiO}_2$  to  $\text{Al}_2\text{O}_3$  which result in a broader spectrum and bending of  $\text{Al}_2\text{O}_3$  at two spectra region;  $594$  and  $639$   $\text{cm}^{-1}$ . This band was not exhibited by textile/ $\text{Al}_2\text{O}_3$ / $\text{TiO}_2$  nanocomposite due to the lack of attachment of  $\text{TiO}_2$  to  $\text{Al}_2\text{O}_3$ , which proves the difference in the structure between textile/ $\text{Al}_2\text{O}_3$ - $\text{TiO}_2$  and textile/ $\text{Al}_2\text{O}_3$ / $\text{TiO}_2$  nanocomposites. For textile/ $\text{Al}_2\text{O}_3$ - $\text{TiO}_2$  nanocomposite, the observed absorption peak at  $639$  and  $694$   $\text{cm}^{-1}$  are assigned to the Al-O bonding vibrations in the  $\text{Al}_2\text{O}_3$ - $\text{TiO}_2$  nanoparticles, respectively (Fig. 2(a), 2(c)). The broad intense bands in the range of  $1200$ – $900$   $\text{cm}^{-1}$  are attributed to cellulose, which appeared less intense in the spectra of the modified cotton (Fig. 2(c), 2(d), 2(e) and 2(f)). The presence of prominent bands at  $1032$  and  $1059$   $\text{cm}^{-1}$  are assigned to the

functional groups of cellulose, namely C–C, C–O and C–O–C stretching vibrations (Fig. 2(b), 2(c), 2(d), 2(e) and 2(f)).<sup>34</sup> The appearance of much weaker bands around 2850–3000  $\text{cm}^{-1}$  correspond to the C–H stretching bands, which confirms the attachment of  $\text{Al}_2\text{O}_3$ - $\text{TiO}_2$  nanoparticles,  $\text{Al}_2\text{O}_3/\text{TiO}_2$  nanoparticles,  $\text{Al}_2\text{O}_3$  nanoparticles and  $\text{TiO}_2$  nanoparticles onto the cotton fabric (Fig. 2(c), 2(d), 2(e) and 2(f)).

### 3.3. Morphology and elemental analysis

The morphology of the prepared nanocomposites observed using FESEM is shown in Fig. 3. From the figure it can be seen that the shape of the nanoparticle attached on the textile is nearly spheroidal. The EDX analysis of textile/ $\text{Al}_2\text{O}_3$  nanocomposite and textile/ $\text{Al}_2\text{O}_3$ - $\text{TiO}_2$  nanocomposite are shown in Fig. 4. Based on the EDX analysis, there are four main elements in textile/ $\text{Al}_2\text{O}_3$  nanocomposite. The elements are carbon (C), aluminium (Al), oxygen (O) and Au (the coating material), with focus on Al and O. The EDX analysis of textile/ $\text{Al}_2\text{O}_3$ - $\text{TiO}_2$  nanocomposite shows five elements, which are Al, Ti, C, O and Au (the coating material). The EDX analysis also shows Al, Ti and O in textile/ $\text{Al}_2\text{O}_3$ - $\text{TiO}_2$  nanocomposite. Based on the FESEM image and EDX analysis, it can be concluded that the textile/ $\text{Al}_2\text{O}_3$  nanocomposite and  $\text{Al}_2\text{O}_3$ - $\text{TiO}_2$ /textile nanocomposite were successfully obtained. Based on Fig. 5 the size of the  $\text{Al}_2\text{O}_3$ - $\text{TiO}_2$  particles attached on the textile were in the range of 50–80 nm, which confirms that these particles are in the nano range.

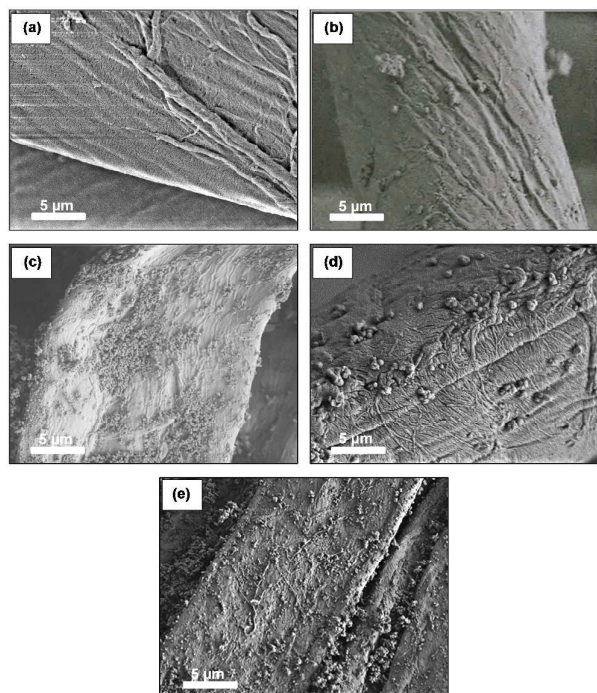


**Fig. 3** FESEM images of (a) textile, (b) textile/ $\text{Al}_2\text{O}_3$  nanocomposite, (c) textile/ $\text{TiO}_2$  nanocomposite, (d) textile/ $\text{Al}_2\text{O}_3$ - $\text{TiO}_2$  nanocomposite, (e) textile/ $\text{Al}_2\text{O}_3/\text{TiO}_2$  nanocomposite.

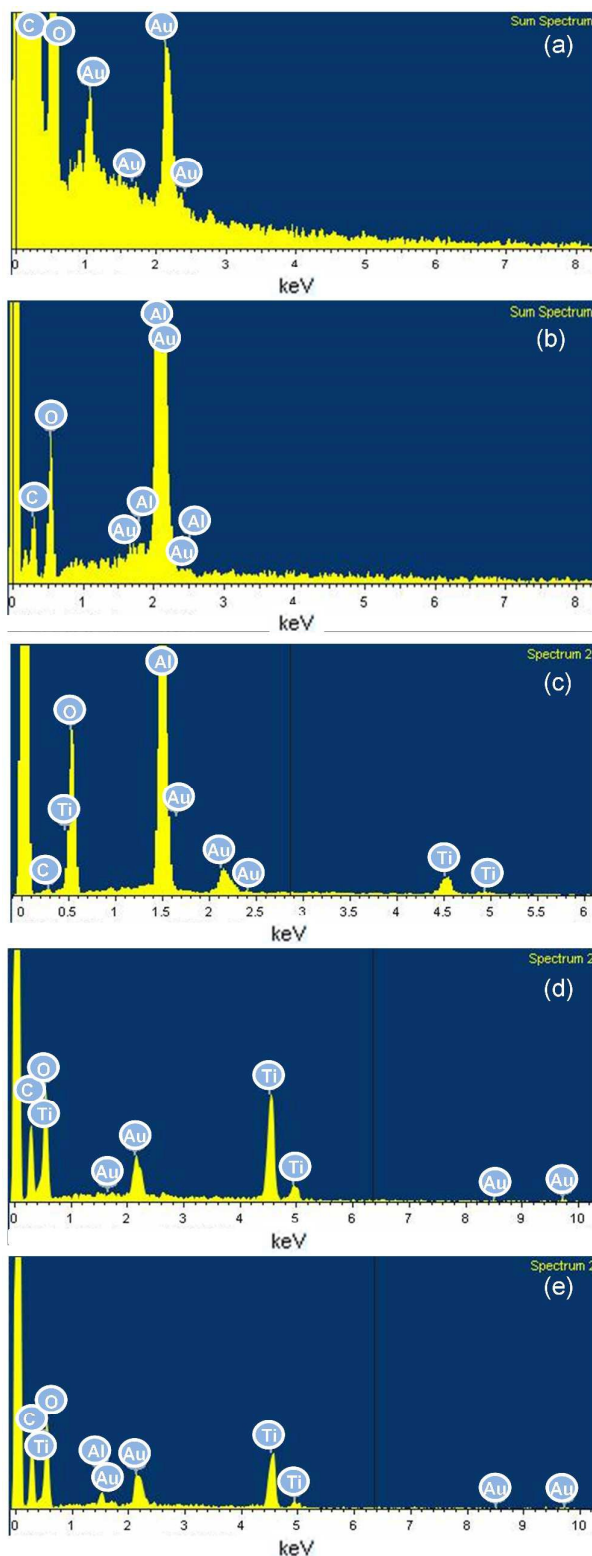


**Fig. 4** EDX analysis of (a) textile, (b) textile/ $\text{Al}_2\text{O}_3$  nanocomposite, (c) textile/ $\text{Al}_2\text{O}_3$ - $\text{TiO}_2$  nanocomposite, (d) textile/ $\text{TiO}_2$  nanocomposite, (e) textile/ $\text{Al}_2\text{O}_3/\text{TiO}_2$  nanocomposite.



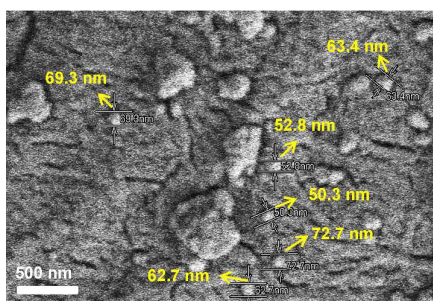


**Fig. 5** The particle size of textile/ $\text{Al}_2\text{O}_3$ - $\text{TiO}_2$  nanocomposite measured from FESEM image.

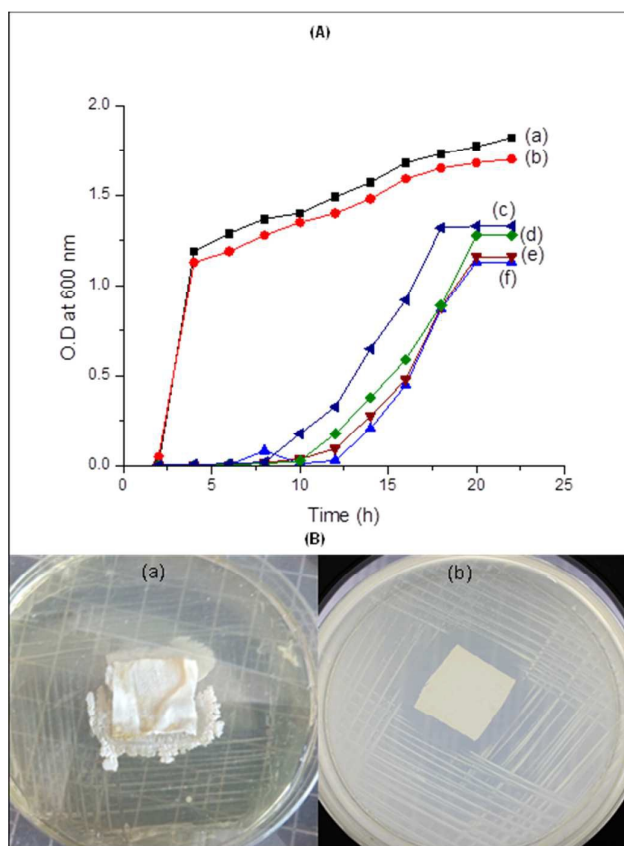


**Fig. 6** Growth of *E. coli* against textile/ $\text{Al}_2\text{O}_3$ - $\text{TiO}_2$  nanocomposite in different concentrations (150, 125, 100 and 75 mmol/L) in (A) liquid medium (LB) (a) culture (b) textile (c) 75 mmole/L (d) 100 mmol/L (e) 125 mmol/L (f) 150 mmol/L and (B) agar medium (a) textile (b) textile/ $\text{Al}_2\text{O}_3$ - $\text{TiO}_2$  nanocomposite.

The FESEM image and EDX analysis of textile/ $\text{Al}_2\text{O}_3$ - $\text{TiO}_2$  nanocomposite and textile/ $\text{Al}_2\text{O}_3$ / $\text{TiO}_2$  nanocomposite are shown in Fig. 3(d), 4(c) and 3(e), 4(e). As for the EDX analysis of textile/ $\text{TiO}_2$  nanocomposite, three elements (Ti, O, and C) can be seen in this nanocomposite. Finally, The FESEM images shown in Fig. 3b, c, d and e display the presence of attachment on the cotton textile after modification. The inset of Fig. 3b, c, d and e show the appearance of frequent roughness and

wrinkles on the textiles' surface, verifying the successful attachment of these nanoparticles onto the cotton textile. The robust surface roughness of textile/ $\text{Al}_2\text{O}_3$  nanocomposite, textile/ $\text{TiO}_2$  nanocomposite, textile/ $\text{Al}_2\text{O}_3$ - $\text{TiO}_2$  nanocomposite and textile/ $\text{Al}_2\text{O}_3$ / $\text{TiO}_2$  nanocomposite are presented in Fig. 3b, c, d and e are due to the growth of nearly spherical nanoparticles on the surface of cotton textile. The inset of Fig. 3b, c, d and e clearly reveal the attachment of these nearly spherical nanoparticles.

From the combination of these results with FTIR results, it can be concluded that this attachment is accrued by the hydrogen bonding between the O-H of the nanoparticles and the O-H of the textiles' surface. This attachment is nearly stable because these nanocomposites washability by distilled water after modification, and the low release of metal oxide from these textile nanocomposites also confirm the stability of this attachment.

### 3.4. Antimicrobial ability

For antimicrobial ability testing, strains of gram-negative bacterium *E. coli* were inoculated in LB medium supplemented with increasing dosages of textile/ $\text{Al}_2\text{O}_3$ - $\text{TiO}_2$  nanocomposite in different concentrations (150, 125, 100 and 75 mmol/L). Increasing concentration of the nanoparticles progressively retarded the growth of *E. coli* (Fig. 6). The concentration of 150 mg/mL of textile/ $\text{Al}_2\text{O}_3$ - $\text{TiO}_2$  nanocomposite was found to be strongly inhibitory for bacteria. The steepness of the growth curve in the logarithmic phase and the final cell concentration were also noticeably lower at the concentration of 125 and 150 mmol/L, as compared with the lower concentrated ones used in this study (75 and 100 mmol/L). The antimicrobial ability comparison between textile/ $\text{Al}_2\text{O}_3$  nanocomposite, textile/ $\text{TiO}_2$  nanocomposite, textile/ $\text{Al}_2\text{O}_3$ - $\text{TiO}_2$  nanocomposite, textile/ $\text{Al}_2\text{O}_3$ / $\text{TiO}_2$  nanocomposite, textile and culture after 14 h is shown in Fig. 7. Textile/ $\text{Al}_2\text{O}_3$  nanocomposite shows mild inhibitory against *E. coli*, even when high concentration (150 mmol/L) was used.

On the other hand, the antimicrobial ability of textile/ $\text{Al}_2\text{O}_3$ - $\text{TiO}_2$  nanocomposite was much higher than those shown by textile/ $\text{TiO}_2$  nanocomposite and textile/ $\text{Al}_2\text{O}_3$ / $\text{TiO}_2$  nanocomposite. Antimicrobial ability has reverse link with bacteria growth therefore, the comparison trend between all samples after 14 h based on Fig. 7 is as follows: textile/ $\text{Al}_2\text{O}_3$ - $\text{TiO}_2$  nanocomposite > textile/ $\text{Al}_2\text{O}_3$ / $\text{TiO}_2$  nanocomposite > textile/ $\text{TiO}_2$  nanocomposite > textile/ $\text{Al}_2\text{O}_3$  nanocomposite > textile > culture. The antimicrobial ability of nanoparticles is also related to the size of the nanoparticles.<sup>15, 17</sup> Smaller-sized nanoparticles have better antimicrobial ability as they possess large surface area. As antibacterial activity is known as the function of the surface area in contact with the microorganisms, therefore, a larger surface area (as in the case of nanoparticles) shows a broader range of probable reactions with bioorganic present on the cell surface.<sup>15</sup> The particle size of  $\text{Al}_2\text{O}_3$ - $\text{TiO}_2$  nanoparticles attached to textile is around 50-80 nm (Fig. 5). This nanocomposite shows higher antimicrobial activity compared to textile/ $\text{Al}_2\text{O}_3$  nanocomposite because of

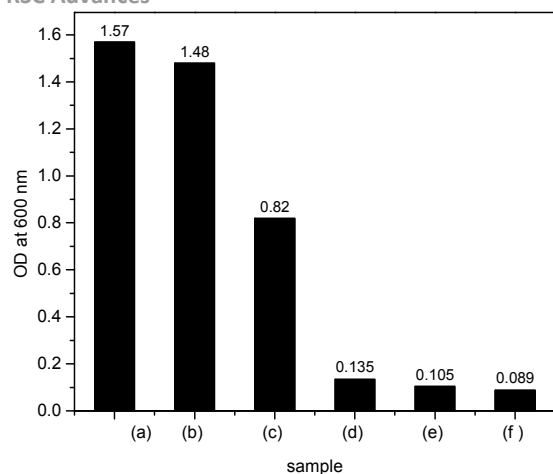


**Fig. 7** Growth E.coli after 14 h shown by: (a) culture, (b) textile, (c) textile/ $\text{Al}_2\text{O}_3$  nanocomposite, (d) textile/ $\text{TiO}_2$  nanocomposite, (e) textile/ $\text{Al}_2\text{O}_3/\text{TiO}_2$  nanocomposite and (f) textile/ $\text{Al}_2\text{O}_3\text{-TiO}_2$  nanocomposite .

the presence of  $\text{TiO}_2$  in the structure of  $\text{Al}_2\text{O}_3\text{-TiO}_2$  nanoparticles, which caused the increase in antimicrobial activity of this nanocomposite. The strong bactericidal effect, as observed with some metal oxides such as  $\text{TiO}_2$ , was not observed in the case of  $\text{Al}_2\text{O}_3$ .<sup>35</sup>

The disruption of cell wall due to the generation of ROS is one of the most important mechanisms behind cell death leading to the strong antimicrobial property of these metal oxides. ROS is very toxic to human body. Consequently, it is evident from this study that  $\text{Al}_2\text{O}_3\text{-TiO}_2$  nanoparticles on textile possess strong antimicrobial properties; high growth inhibition was noticed at high concentration of nanoparticles of up to 100 mmol/L. These observations are pertinent to the ecotoxicity of textile/ $\text{Al}_2\text{O}_3\text{-TiO}_2$  nanocomposite against bacteria. This laboratory-scale study suggests that textile/ $\text{Al}_2\text{O}_3\text{-TiO}_2$  is strongly toxic to microorganisms in the environment.

### 3.5. Radical scavenging ability

The amount of radical scavenging ability of textile/ $\text{Al}_2\text{O}_3$  nanocomposite, textile/ $\text{Al}_2\text{O}_3/\text{TiO}_2$  nanocomposite, textile/ $\text{Al}_2\text{O}_3\text{-TiO}_2$  nanocomposite, textile/ $\text{TiO}_2$  nanocomposite and textile as the control is calculated by eqn (1) and shown in Table 3.

**Table 3** Radical scavenging ability of textile/ $\text{TiO}_2$ , textile/ $\text{Al}_2\text{O}_3$  nanocomposite, textile/ $\text{Al}_2\text{O}_3/\text{TiO}_2$  nanocomposite and textile/ $\text{Al}_2\text{O}_3\text{-TiO}_2$  nanocomposite.

Samples	Absorbance of the samples ( $A_s$ )	Radical scavenging ability (% $S_a$ )
Textile/ $\text{Al}_2\text{O}_3\text{-TiO}_2$ nanocomposite	0.623	38.2%
Textile/ $\text{Al}_2\text{O}_3/\text{TiO}_2$ nanocomposite	0.654	35.5%
Textile/ $\text{Al}_2\text{O}_3$ nanocomposite	0.660	35.0%
Textile/ $\text{TiO}_2$ nanocomposite	1.015	0.2%

The comparison of radical scavenging ability between negative and positive samples is also reported in Table 3. Based on the Table 3, textile/ $\text{Al}_2\text{O}_3\text{-TiO}_2$  nanocomposite has the highest radical scavenging ability (38.2 %), due to the structure of this nanocomposite. The radical scavenging ability of textile/ $\text{Al}_2\text{O}_3$  nanocomposite and textile/ $\text{Al}_2\text{O}_3/\text{TiO}_2$  nanocomposite are 35 and 35.5%, respectively. Although textile/ $\text{TiO}_2$  nanocomposite has strong antimicrobial ability, it did not show any radical scavenging ability. On the other hand, textile/ $\text{Al}_2\text{O}_3\text{-TiO}_2$  nanocomposite has shown high radical scavenging ability.

### 3.6. Cytotoxicity

The fluorescent microscopy image of human skin fibroblasts (HSF) growth on the treatment of all samples, 2 days post seeding can be seen in Fig. 8, respectively. For both textile/ $\text{Al}_2\text{O}_3$  nanocomposite and textile/ $\text{Al}_2\text{O}_3\text{-TiO}_2$  nanocomposite, the cell culture indicates improved cell viability and proliferation. No discernible difference can be seen between these two types of textile nanocomposite. This result confirms the radical scavenger ability of these nanocomposites. In the case of textile/ $\text{Al}_2\text{O}_3/\text{TiO}_2$  nanocomposite, the cell culture shows cell viability lower than previous nanocomposite. On the other hand textile/ $\text{TiO}_2$  nanocomposite does not show any cell viability because it cannot act as radical scavenger and ROS could have been distributed through the cell wall of HSF.

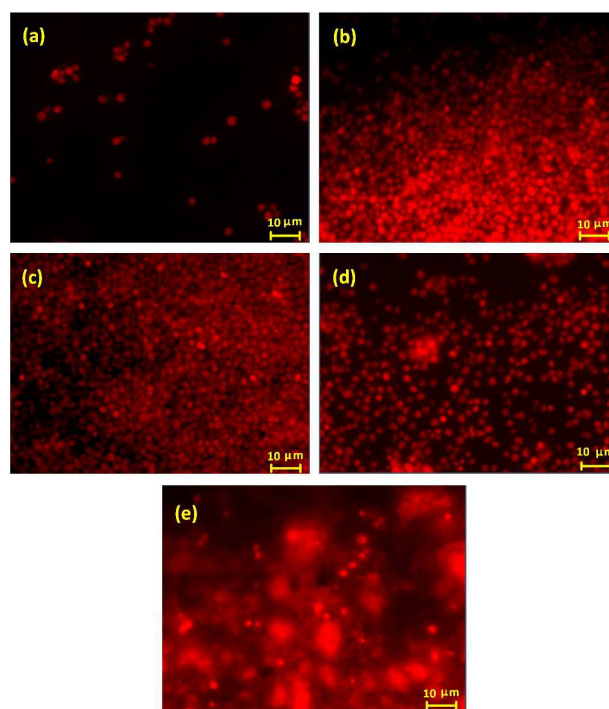


**Fig. 8** The fluorescent microscopy image of human skin fibroblasts (HSF) growth on the different treatment: (a) without treatment, (b) textile/ $\text{Al}_2\text{O}_3$  nanocomposite, (c) textile/ $\text{Al}_2\text{O}_3\text{-TiO}_2$  nanocomposite, (d) textile/ $\text{Al}_2\text{O}_3/\text{TiO}_2$  nanocomposite, (e) textile/ $\text{TiO}_2$  nanocomposite.

**Table 4** The release of the inorganic content from the textile of textile/ $\text{Al}_2\text{O}_3$  nanocomposite, textile/ $\text{Al}_2\text{O}_3/\text{TiO}_2$  nanocomposite, textile/ $\text{Al}_2\text{O}_3\text{-TiO}_2$  nanocomposite, textile/ $\text{TiO}_2$  nanocomposite.

Samples	Inorganic release amount ( $\mu\text{g/L}$ )
Textile/ $\text{Al}_2\text{O}_3\text{-TiO}_2$ nanocomposite	9.831
Textile/ $\text{Al}_2\text{O}_3/\text{TiO}_2$ nanocomposite	14.071
Textile/ $\text{Al}_2\text{O}_3$ nanocomposite	7.160
Textile/ $\text{TiO}_2$ nanocomposite	11.340

The release of the inorganic content from the textile of textile/ $\text{Al}_2\text{O}_3$  nanocomposite, textile/ $\text{Al}_2\text{O}_3/\text{TiO}_2$  nanocomposite, textile/ $\text{Al}_2\text{O}_3\text{-TiO}_2$  nanocomposite, textile/ $\text{TiO}_2$  nanocomposite is shown in Table 4. Based on Table 4, textile/ $\text{Al}_2\text{O}_3\text{-TiO}_2$  nanocomposite and textile/ $\text{Al}_2\text{O}_3$  have the lowest amount of inorganic release from textile. Therefore, the attachment of these nanoparticles of textile is almost stable.

The application of surface modification of textile is an accepted technique to improve the initial antimicrobial, radical scavenger and biocompatibility of textile/ $\text{Al}_2\text{O}_3\text{-TiO}_2$  nanocomposite.  $\text{Al}_2\text{O}_3\text{-TiO}_2$  nanoparticles can be used to provide localized high wound healing to the textile. With the intention to increase both antimicrobial ability and nontoxicity of biological agents, the textile/ $\text{Al}_2\text{O}_3\text{-TiO}_2$  nanocomposite is suggested to be used as wound dressing. This antimicrobial and non-toxic wound dressing can improve wound healing process.

#### 4. Conclusions

Textile/ $\text{Al}_2\text{O}_3$  nanocomposite, textile/ $\text{Al}_2\text{O}_3/\text{TiO}_2$  nanocomposite, textile/ $\text{TiO}_2$  nanocomposite and textile/ $\text{Al}_2\text{O}_3\text{-TiO}_2$  nanocomposite were successfully synthesized via the sol gel method and attachment on textile. The role of  $\text{Al}_2\text{O}_3\text{-TiO}_2$  in antimicrobial and radical scavenging properties was studied through in-depth characterizations at room temperature. The presence of  $\text{TiO}_2$  in  $\text{Al}_2\text{O}_3\text{-TiO}_2$  nanoparticles is found to increase the antimicrobial ability of textile/ $\text{Al}_2\text{O}_3\text{-TiO}_2$  nanocomposite. The textile/ $\text{Al}_2\text{O}_3\text{-TiO}_2$  nanocomposite shows strong antimicrobial activity and the ability to scavenge ROS. The outstanding features of the results indicate that this easy and environmental-friendly preparation method can be used as an effective wound dressing.

#### Acknowledgements

The authors gratefully acknowledge funding from Universiti Teknologi Malaysia (UTM) through Research University Grant. D.H.B. Wicaksono acknowledges funding from RU Grant 05H32. The authors also would like to thank Prof. Dr. Fahrul Zaman Huyop (Faculty of Biosciences and Medical Engineering, UTM) for his support in the antimicrobial analysis.

#### References

- H. Kim, I. Makin, J. Skiba, A. Ho, G. Housler, A. Stojadinovic and M. Izadjoo, *Open Microbiol. J.*, 2014, **8**, 15-21.
- J. Banerjee, P. D. Ghatak, S. Roy, S. Khanna, E. K. Sequi, K. Bellman, B. C. Dickinson, P. Suri, V. V. Subramaniam, C. J. Chang and C. K. Sen, *PLoS One*, 2014, **9**, e89239.
- R. Jayakumar, M. Prabakaran, P. S. Kumar, S. Nair and H. Tamura, *Biotechnol. Adv.*, 2011, **29**, 322-337.
- C. K. Bower, J. E. Parker, A. Z. Higgins, M. E. Oest, J. T. Wilson, B. A. Valentine, M. K. Bothwell and J. McGuire, *Colloids Surface B*, 2002, **25**, 81-90.
- S. J. Soenen, P. Rivera-Gil, J.-M. Montenegro, W. J. Parak, S. C. De Smedt and K. Braeckmans, *Nano Today*, 2011, **6**, 446-465.
- L. Yildirimer, N. T. K. Thanh, M. Loizidou and A. M. Seifalian, *Nano Today*, 2011, **6**, 585-607.
- X. Ren, L. Kou, H. B. Kocer, C. Zhu, S. Worley, R. Broughton and T. Huang, *Colloids Surface A*, 2008, **317**, 711-716.
- P. Kaushik and A. Malik, *Environ. Int.*, 2009, **35**, 127-141.
- J. V. Edwards and T. L. Vigo, *Bioactive fibers and polymers*, Oxford University Press, 2001.
- C. G. Gebelein and C. E. Carraher, *Biotechnology and bioactive polymers*, Springer, 1994.
- M. Montazer and M. G. Afjeh, *J. Appl. Polym. Sci.*, 2007, **103**, 178-185.
- R. Dastjerdi, M. Mojtahedi, A. Shoshtari and A. Khosroshahi, *J. Text. I.*, 2010, **101**, 204-213.
- N. Ladhari, M. Baouab, A. Ben Dekhil, A. Bakhrout and P. Niquette, *J. Text. I.*, 2007, **98**, 209-218.
- J. M. Miller and L. J. Lakshmi, *J. Phys. Chem. B.*, 1998, **102**, 6465-6470.
- H. Gleiter, *Acta. Mater.*, 2000, **48**, 1-29.
- A. Curtis and C. Wilkinson, *Trends Biotechnol.*, 2001, **19**, 97-101.
- X. Qiu, M. Miyauchi, K. Sunada, M. Minoshima, M. Liu, Y. Lu, D. Li, Y. Shimodaira, Y. Hosogi, Y. Kuroda and K. Hashimoto, *ACS Nano*, 2012, **6**, 1609-1618.
- S. Makhluif, R. Dror, Y. Nitzan, Y. Abramovich, R. Jelinek and A. Gedanken, *Adv. Funct. Mater.*, 2005, **15**, 1708-1715.
- P. Holister, J. W. Weener, V. C. Romas and T. Harper, *Nanoparticles: Technology white papers 3*, Scientific Ltd, 2003.
- R. Brayner, R. Ferrari-Iliou, N. Brivois, S. Djediat, M. F. Benedetti and F. Fiévet, *Nano Lett.*, 2006, **6**, 866-870.
- P. Zieliński, R. Schulz, S. Kaliaguine and A. Van Neste, *J. Mater. Res.*, 1993, **8**, 2985-2992.
- P. Ganguly and W. J. Poole, *Mat. Sci. Eng. A*, 2003, **352**, 46-54.
- R. Dastjerdi and M. Montazer, *Colloid Surface B*, 2010, **79**, 5.
- A. Nilghaz, D. H. Wicaksono, D. Gustiono, F. A. A. Majid, E. Supriyanto and M. R. A. Kadir, *Lab Chip*, 2012, **12**, 209-218.
- J. Li, Y. Pan, C. Xiang, Q. Ge and J. Guo, *Ceram. Int.*, 2006, **32**, 587-591.
- D. N. Williams, S. H. Ehrman and T. R. P. Holoman, *J. Nanobiotechnology*, 2006, **4**, 3.
- Z. Yaping, Y. Wenli, W. Dapu, L. Xiaofeng and H. Tianxi, *Food Chem.*, 2003, **80**, 115-118.
- G. Mohammad, V. K. Mishra and H. Pandey, *Dig. J. Nanomater. Biost.*, 2008, **3**, 159-162.
- S. Hoffmann, S. T. Norberg, and M. Yoshimura, *J. Electroceram.*, 2006, **16**, 327-330.
- R. W. Grimes and J. Pilling, *J. Mater. Sci.*, 1994, **29**, 2245-2249.
- H. Bian, Y. Yang, Y. Wang, W. Tian, H. Jiang, Z. Hu, W. Yu, J. Mater. Sci. Technol., 2013, **29**, 429-433.
- W. Mozgawa, M. Król, and T. Bajda, *J. Mol. Struct.*, 2009, **924**, 427-433.

- 33 P. Padmaja, G. Anilkumar, P. Mukundan, G. Aruldhas and K. Warriar, *Int. J. Inorg. Mater.*, 2001, **3**, 693-698.
- 34 K. Kavkler, N. Gunde-Cimerman, P. Zalar and A. Demšar, *Polym. Degrad. Stabil.*, 2011, **96**, 574-580.
- 35 A. Besinis, T. De Peralta and R. D. Handy, *Nanotoxicology*, 2014, **8**, 1-16.

